



# Gas evolution from cathode materials: A pathway to solvent decomposition concomitant to SEI formation



Katie L. Browning, Loïc Baggetto, Raymond R. Unocic, Nancy J. Dudney, Gabriel M. Veith\*

Materials Science and Technology Division, Oak Ridge National Laboratory, Oak Ridge, TN 37831, USA

## HIGHLIGHTS

- Surface chemistry of  $\text{LiCoO}_2$  will influence catalytic decomposition of electrolyte molecules.
- $\text{CO}_2$  solubility affected by solvent composition with solubilities up to  $0.02 \text{ g CO}_2 \text{ mL}^{-1}$ .
- Alternative to electrochemical SEI formation that may mediate cell lifetime.

## ARTICLE INFO

### Article history:

Received 25 February 2013

Received in revised form

22 March 2013

Accepted 23 March 2013

Available online 1 April 2013

### Keywords:

Li-ion safety

Gas evolution

Electrolyte decomposition

Coulombic losses

## ABSTRACT

This work reports a method to explore the catalytic reactivity of electrode surfaces toward the decomposition of carbonate solvents [ethylene carbonate (EC), dimethyl carbonate (DMC), and EC/DMC]. We show that the decomposition of a 1:1 wt% EC/DMC mixture is accelerated over certain commercially available  $\text{LiCoO}_2$  materials resulting in the formation of  $\text{CO}_2$  while over pure EC or DMC the reaction is much slower or negligible. The solubility of the produced  $\text{CO}_2$  in carbonate solvents is high ( $0.025 \text{ g mL}^{-1}$ ) which masks the effect of electrolyte decomposition during storage or use. The origin of this decomposition is not clear but it is expected to be present on other cathode materials and may affect the analysis of SEI products as well as the safety of Li-ion batteries.

© 2013 Elsevier B.V. All rights reserved.

## 1. Introduction

Controlling the electrolyte–electrode interface is one of the critical challenges associated with developing stable and reliable energy storage technologies. To date most academic scientists and reports in the peer reviewed literature have focused on electrochemical reactions at the interface such as those involved in the formation of a passivating solid–electrolyte interphase (SEI) [1–3]. Extensive SEI formation will result in a significant reduction of cell capacity due to the consumption of Li or an increase in cell impedance due to the passivating nature of the SEI layer [3].

Compared to electrochemical reactions there has been relatively little exploration of the chemical reactivity of electrode surfaces with electrolyte components. Chemical reactions are arguably as important as electrochemical reactions [4]. Indeed chemical reactions could consume electrolyte resulting in a decrease in cell performance similar to excessive SEI formation, but can also lead to the formation of a large volume of gas causing cells to rupture [4].

Such cell failures have been mentioned in the literature but rarely investigated in extensive detail by the academic community, despite the critical importance of cell safety in the nascent battery industry [5,6]. The studies that have been performed on gas evolution have focused on evolution as a function of potential or cycling but not the basic uncycled material [7–10].

The catalytic properties of metal oxides have been the subject of extensive studies from the heterogeneous catalysis community. The activity of these surfaces depends highly on synthesis conditions, impurities, surface area, and storage/processing conditions all of which could affect electrode performance and stability. Furthermore, it is well known that under atmospheric conditions metal oxides such as  $\text{TiO}_2$ ,  $\text{SiO}_2$  and  $\text{SnO}_2$  are covered with 2–3 monolayers of strongly bound water [11–14]. The structure and concentration of water on an oxide surface depends on processing conditions. In general this water persists to high temperatures ( $>300^\circ\text{C}$ ) and under vacuum. Indeed, ultra high vacuum surface science studies have to go to extreme processing conditions ( $>800^\circ\text{C}$  with ion bombardment) to create metal oxide surfaces without water [15]. It is likely that high surface area battery electrode materials introduce significant concentrations of strongly

\* Corresponding author.

E-mail address: [veithgm@ornl.gov](mailto:veithgm@ornl.gov) (G.M. Veith).

bound water to cells with low volumes of electrolyte. Since water is known to affect electrolyte chemistry and electrode stability the presence of strongly bound water could have a major effect on cell performance. Another variable which may affect chemical reactivity is the selective segregation of chemical components to the surface of the electrode during cell operation. For example, Li could be drawn to the electrode surface by reaction with  $\text{CO}_2$  forming a basic  $\text{Li}_2\text{CO}_3$  surface coating which may react differently than a pure lithium metal oxide surface. Indeed, recent studies have shown that the segregation of species, such as Ni, to the surface of a cathode will significantly influence the performance of the electrode material [16].

In this work we present a process to explore the intrinsic chemical reactivity of battery materials ( $\text{LiCoO}_2$ ) with respect to the carbonate components employed in typical Li-ion electrolyte solvent mixtures (ethylene carbonate/dimethyl carbonate). These measurements were performed without electrochemical cycling which may mask the chemical reactivity of the electrode surface. The results show that the activity of different electrodes varies significantly depending on electrode chemistry as well as the ratio of the carbonate molecules. These variables should be studied in greater detail with the advent of new battery chemistries and electrolytes.

## 2. Experimental

### 2.1. Materials

Three different  $\text{LiCoO}_2$  powders were selected for this work based on their compositions from ICP measurements. The  $\text{LiCoO}_2$  powders were obtained from Cerac (99.5%) – Sample A, Targray (L106 grade) – Sample B, and Alfa Aesar (98%) – Sample C, and were dried under vacuum for 12 h prior to use. High purity ethylene carbonate (EC, Sigma Aldrich – 99% anhydrous) was used as received while dimethyl carbonate (DMC, Sigma Aldrich – >99% anhydrous) was dried over molecular sieves for several weeks. A 50:50 wt% mixture of EC/DMC was prepared from these parent reagents and dried for several weeks over molecular sieves. The water content was determined to be less than 2 ppm by Karl Fisher titration (Metler Toledo – C20 coulometric titrator).

### 2.2. Pressure cell measurements

The pressure cells were composed of 316 stainless steel tubing and Swagelok components connected to a PX309 series pressure transducer (0–100 psia, Omega Engineering), Fig. S1. After construction the cells were leak tested by evacuating the cells and back filling with ~50 psia of He gas. The pressure of the cell was monitored over 24 h to ensure that none of the He leaked out of the cell. After the leak test 2 g of  $\text{LiCoO}_2$  powder was placed in the bottom of the homemade pressure cell along with 1 g of electrolyte added from above in an argon filled glove box. The cells were sealed and heated to 54 °C in a constant temperature oven. The pressure in the cell was monitored as a function of time. The volume of the cell was estimated gravimetrically by the application of the Ideal Gas Law: cells were evacuated and weighed or evacuated and charged with 95 psia of  $\text{CO}_2$  and then weighed to the closest mg.

### 2.3. $\text{CO}_2$ solubility

The solubility of  $\text{CO}_2$  in EC, DMC, and EC/DMC was estimated using a modified pressure cell, Fig. S2. The volumes of the cells were estimated gravimetrically as before. One half of the cell was charged with 95 psia of  $\text{CO}_2$  while the other half of the cell was filled with 2 mL of electrolyte under Ar in an Ar filled glove box. A

valve between the two halves of the cell was opened allowing the pressure to equilibrate instantly. The pressure of the cell was then monitored as a function of time to quantify the amount of  $\text{CO}_2$  dissolved in the carbonate solutions. Solubility was measured at room temperature (18 °C), after heating to 54 °C, and then again at 18 °C to ensure reproducibility. WARNING:  $\text{CO}_2$  and ethylene carbonate mixtures when cooled form a supercooled fluid that when disturbed will violently evolve gas. Vent with suitable protection and containment.

### 2.4. Materials characterization

Nitrogen BET measurements were performed using an Autosorb 1C (Quantachrome Instruments) at 77 K. Due to the low surface area of  $\text{LiCoO}_2$  approximately 10 g of powder was used for the measurements after degassing at 300 °C for 8 h. The structure and morphology of the  $\text{LiCoO}_2$  materials were characterized using a Hitachi S-4800 scanning electron microscope (SEM). X-ray photoelectron spectroscopy (XPS) high resolution data were collected using a PHI 3056 spectrometer with an Al anode source operated at 15 kV and an applied power of 350 W. Elemental analysis was performed using a Thermo Jarrell Ash IRIS Inductively Coupled Plasma (ICP) Optical Emission Spectrometer (OES). ~0.05 g of  $\text{LiCoO}_2$  was dissolved in freshly prepared aqua-regia (3:1 mixture of hydrochloric acid and nitric acid) for analysis and diluted with a 5%  $\text{HNO}_3$  solution prepared in deionized water (18.3 MΩ). The resulting solution was diluted to obtain a solution in the linear sensitivity range of the ICP. ICP standards were prepared by the serial dilution of Li and Co standards purchased from Alfa-Aesar. Analysis of the gas products formed in the pressure cells was performed using a Ametek Dymaxion Mass Spectrometer (0–200 amu). Surface acidity/basicity was estimated by measuring the equilibrium pH, with an Orion pH electrode, of approximately 0.5 m<sup>2</sup> of material in 25 mL of deionized water degassed by boiling and cooled to room temperature under flowing  $\text{N}_2$ . To further estimate the basicity of the  $\text{LiCoO}_2$  powders  $\text{NH}_3$  Temperature Probed Desorption (TPD) measurements were performed. The 1 m<sup>2</sup> of sample was heated to 125 °C in flowing He (50 sccm) for 1 h then cooled to 22 °C to remove weakly bound water. The sample was reacted with a 5%  $\text{NH}_3$ /He mixture for 30 min (50 sccm). The sample was then heated under 50 mL min<sup>-1</sup> He at 100 °C h<sup>-1</sup> to 400 °C and evolved  $\text{NH}_3$  was followed using the mass spectrometer. Fourier Transform Infrared (FTIR) spectroscopy data was measured with a  $\text{N}_2$  purged FTIR Spectrometer (BioRad 575C), equipped with a room temperature Deuterated Triglycine Sulfate (DTGS) detector and KBr beamsplitter, controlled with WinIR-Pro software. Approximately 1.5 mg of  $\text{LiCoO}_2$  was ground together with 0.6 g of KBr (Optical grade powder) in an agate mortar until well mixed. Then 0.15 g of the  $\text{LiCoO}_2$ /KBr mixture was pressed into a thin 1/2" diameter pellet at 10,000 lbs of pressure. A 0.15 g pellet of ground KBr was used to determine the background. Spectra of the pellets were recorded with 4 cm<sup>-1</sup> resolution. X-ray diffraction data were collected using a Scintag Pad V diffractometer utilizing a  $\text{CuK}\alpha$  source. Samples were randomized on a zero-background polycarbonate holder prior to data collection.

### 2.5. Electrochemical characterization

Electrodes were fabricated using 86 wt% active material intimately mixed with 8 wt% polyvinylidene fluoride (PVdF) (Sigma Aldrich), 4 wt% C65 carbon black (Timcal) and 2 wt% graphite (Timcal) in 1-methyl-2-pyrrolidinone. The mixtures were cast onto battery grade aluminum foil left to dry under vacuum/heating to 100 °C for 1 h. The resulting material was punched to form 1 cm diameter disks and assembled in an Ar filled glove box using CR2032 coin cells (Hohsen, Japan) with a Celgard 2500 separator,

1.2 M LiPF<sub>6</sub> in 1:1 wt% ethylene carbonate/dimethyl carbonate (EC/DMC) (Novolyte) electrolyte, and a Li foil counter electrode (0.75 mm thick, Alfa Aesar). Cycling was performed using a Maccor battery tester, model 4000, at a rate of C/5 between 3 V and 4.2 V.

### 3. Results and discussion

It is important to note that the materials used in this study were not selected based on electrochemical performance and the choices are not an indication of favoritism toward products of particular manufacturers. Instead the powders were selected to characterize the variability in chemical reactivity of nominally the same cathode material. A summary of the measured materials properties is listed in Table 1. The ICP data show wide variation in the Li:Co ratio of these three materials: Sample A  $1.02 \pm 0.02$ , Sample B  $1.09 \pm 0.04$ , and Sample C  $-0.89 \pm 0.02$  respectively indicating that the materials were either stoichiometric, Li-rich, or Li-deficient. The range of stoichiometries are consistent with different fabrication process and starting reagents [17–19]. BET surface area analysis indicated that the materials were completely non-porous (using the *t*-method) and with low surface areas of  $0.2 \text{ m}^2 \text{ g}^{-1}$  (Sample C),  $0.9 \text{ m}^2 \text{ g}^{-1}$  (Sample B), and  $1.0 \text{ m}^2 \text{ g}^{-1}$  (Sample A). Fig. 1 shows representative SEM data collected on these materials. In all cases there is a distribution in particle sizes and exposed surfaces. The Sample A and Sample C powders have a faceted surface morphology whereas the Sample B materials have a smoother surface morphology. The refined lattice parameters, presented in Table 1, are in good agreement with reported lattice parameters for LiCoO<sub>2</sub> (i.e.  $a = \sim 2.816 \text{ \AA}$  and  $c = \sim 14.05 \text{ \AA}$ ) [20].

Pressure cell measurements were performed at  $54^\circ \text{C}$  to accelerate reaction kinetics, and as demonstrated later reduce the solubility of CO<sub>2</sub> in the solvent. Representative experimental data for the three powders exposed to a 1:1 wt% mixture of EC/DMC is shown in Fig. 2A. From this data it is clear that there is a significant evolution of gaseous products as a function of time for the EC/DMC exposed to the Sample A powder. In contrast there is relatively little gas evolution from the Sample B and C powders at the same temperature. To identify which electrolyte solvent component reacts, experiments were performed where the Sample A powder is reacted with pure EC or pure DMC, Fig. 2B and C respectively. Notice

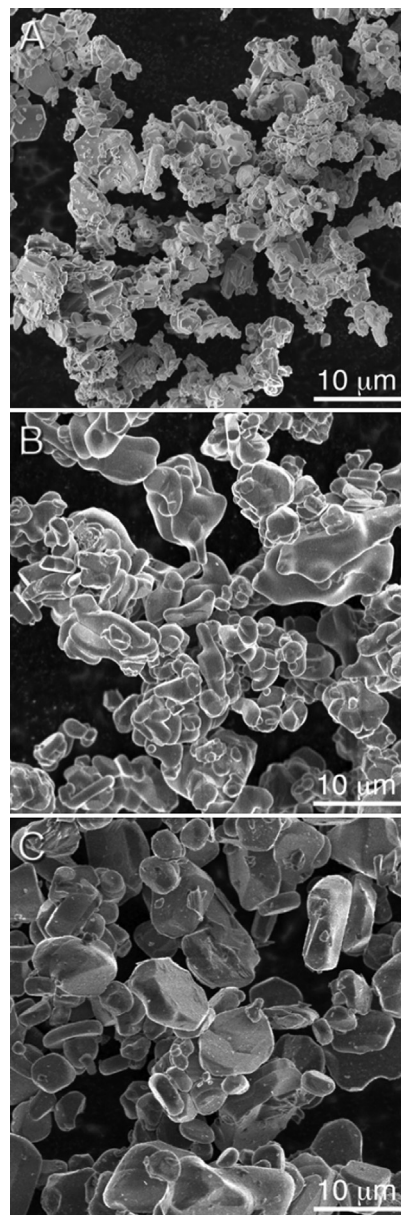


Fig. 1. SEM images of LiCoO<sub>2</sub> powders used in this study.

**Table 1**  
Summary of characterization data obtained for LiCoO<sub>2</sub> samples used in this study.

	Sample A	Sample B	Sample C
Li:Co atomic ratio	$1.02 \pm 0.02$	$1.09 \pm 0.04$	$0.89 \pm 0.02$
BET surface area ( $\text{m}^2 \text{ g}^{-1}$ )	1.0	0.9	0.2
Lattice parameters			
<i>a</i> (Å)	2.815	2.816	2.816
<i>c</i> (Å)	14.0508	14.0539	14.0517
XPS surface species (at%)			
Li	6.1	7.0	11.0 <sup>a</sup>
Co	17.8	15.2	10.9
O	55.0	52.0	56.1
C	15.6	24.1	19.8
Na	5.5	1.4	0.5
Ca		0.3	0.8
S			0.7
Cl			0.2
pH	9.4	9.2	11.2
CO <sub>2</sub> solubility ( $\text{g mL}^{-1}$ )	$20^\circ \text{C}$	$54^\circ \text{C}$	
EC	Solid	0.002	
DMC	0.012	0.005	
EC/DMC (1:1 wt%)	0.025	0.012	

<sup>a</sup> Li<sub>2</sub>CO<sub>3</sub> dominated spectra.

the initial pressures in all these measurements varies due to the different vapor pressures between EC, DMC and EC/DMC. Interestingly, there is very little gas evolution as a function of time in the pure solvents, which indicates that the reactivity of EC/DMC is fundamentally different possibly due to the molecular interactions between these two molecules in the liquid phase.

To identify the gas products formed, mass spectroscopy (MS) measurements were performed, Fig. 3. From these measurements several gaseous species are identified. The He and Ar signals are due to the carrier gas in the MS and the Ar that fills the pressure cells from the glove box respectively. The N<sub>2</sub> and O<sub>2</sub> were introduced from the sampling needle and are due to air as confirmed with by reference studies. The residual species are all due to the decomposition products formed in the cell and consist of CH<sub>x</sub> fragments, OCH<sub>3</sub> (29 amu), CH<sub>3</sub>CO<sub>2</sub> (59 amu), and CO<sub>2</sub> (44 amu). All of these species originate from the carbonate electrolyte. The exact concentration of these species is difficult to quantify based on their different fragmentation efficiencies in the MS, but based on

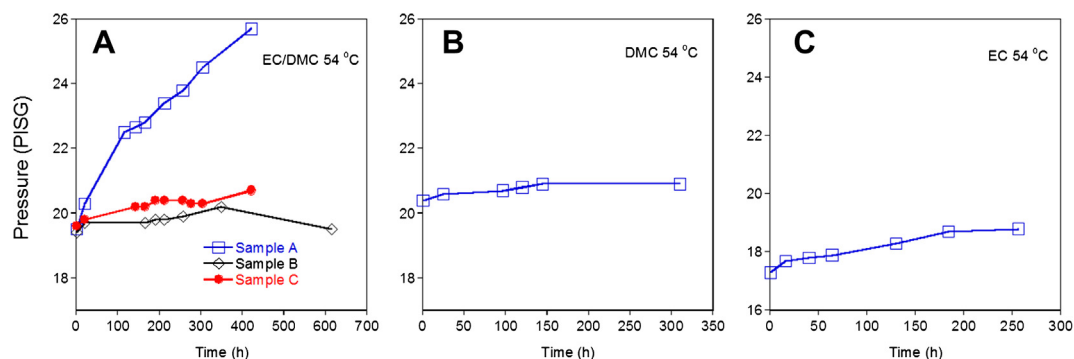


Fig. 2. Pressure measurements in (A) 50:50 wt% EC/DMC, (B) EC; (C) DMC at 54 °C as a function of time.

experience, and the solubility data, discussed below, the largest gas product is CO<sub>2</sub>.

A significant reduction in pressure was observed when the cells were cooled due to the natural relationship between pressure and temperature. However, for the Sample A cells with EC/DMC the change in pressure was several PSI larger than what was observed for reference experiments with pure gas indicating that some of the formed gas products were dissolved in the residual solvent. To investigate this phenomenon the solubility of CO<sub>2</sub> was measured in the carbonate solvents using the procedure described in the experimental section, Table 1. Based on the change in pressure the solubility of CO<sub>2</sub> in EC/DMC at 20 °C is estimated to be 0.025 g of CO<sub>2</sub> mL<sup>-1</sup> of 1:1 wt% EC/DMC. At 54 °C the solubility of CO<sub>2</sub> was much lower (0.012 g of CO<sub>2</sub> mL<sup>-1</sup>). For comparison the solubility of CO<sub>2</sub> in EC after heating and cooling to RT (where it is a solid) is estimated to be 0.002 g of CO<sub>2</sub> mL<sup>-1</sup> EC while the solubility of CO<sub>2</sub> in DMC is found to be 0.012 g of CO<sub>2</sub> mL<sup>-1</sup> at room temperature and 0.005 g of CO<sub>2</sub> mL<sup>-1</sup> at 54 °C. This variation in CO<sub>2</sub> solubility follows previously reported trends [21–23]. However the CO<sub>2</sub> dissolved in EC/DMC is slightly higher than what has been reported previously [23]. We note that the methodologies used in our study and previous studies are different in that previous studies are based on dissolving CO<sub>2</sub> and then displacing it with Ar gas [23]. It is unknown if all the CO<sub>2</sub> is displaced in this method which would affect CO<sub>2</sub> solubility.

This solubility data has several implications for the chemical reactivity of electrolytes. First the solubility of CO<sub>2</sub> in the EC/DMC mixture is significantly greater than a predicted 50/50 mixture would have based on the solubilities of the pure carbonates. This large solubility is probably correlated with the changes in activity measurements shown in Fig. 2A and is likely resulting from the molecular interactions between the two carbonate molecules. Second, a high solubility infers that most of the CO<sub>2</sub> produced at 54 °C is dissolved in the residual solvent upon cooling which would affect the gas sampled in the MS. Finally measurements at room temperature would yield very little information since most of the gas produced would be dissolved in the electrolyte masking the true reactivity of the cathode surface.

It would be tempting to simply correlate the chemical activity with the simple variation in Li:Co chemistry between the various cathode samples. However, surface reactivity is complex, therefore extensive characterization studies were performed and summarized here. Specific emphasis was focused on factors which are known to affect heterogeneous catalysts [24].

### 3.1. Surface area considerations

Often activity increases as a function of surface area. However, the changes observed in activity of these cathodes do not correspond with differences in surface areas, Table 1. Indeed the surface

area of the Sample B (inactive) is nearly identical to the active Sample A powder (0.9 vs. 1.0 m<sup>2</sup> g<sup>-1</sup> respectively).

### 3.2. Surface chemistry considerations

XPS studies were performed and are summarized in Fig. 4. The Co2p, 3s, and 3p data are all consistent with the presence of mainly Co<sup>3+</sup> ions as expected for LiCoO<sub>2</sub>. The presence of small shake up lines in the Co 2p data (785.5 eV) indicates that there is a small concentration of Co<sup>2+</sup> on the surface of the samples, though the relative amounts are fairly constant. C1s data collected on these powders reveals the presence of C–C and C–H type species due to adventitious carbons. There are small concentrations of C=O species on the Sample A and Sample B materials, and a high concentration of –CO<sub>3</sub> type species (290 eV) on the Sample C powder. This –CO<sub>3</sub> is attributed to the presence of Li<sub>2</sub>CO<sub>3</sub> on the cathode surface by comparing with the spectra of pure Li<sub>2</sub>CO<sub>3</sub> and supported by the weak shoulder in the Li1s data at 55.5 eV [25]. The O1s data shows two O species on the surface of each cathode powder. The low energy peak (~529.5 eV) is attributed to lattice oxygen. The high energy peak (~531.5 eV) is attributed to strongly bound surface water/hydroxyls, as discussed in the introduction, or –CO<sub>3</sub> surface impurities. However, aside from the residual Li<sub>2</sub>CO<sub>3</sub> the chemistry of these oxides is surprisingly similar.

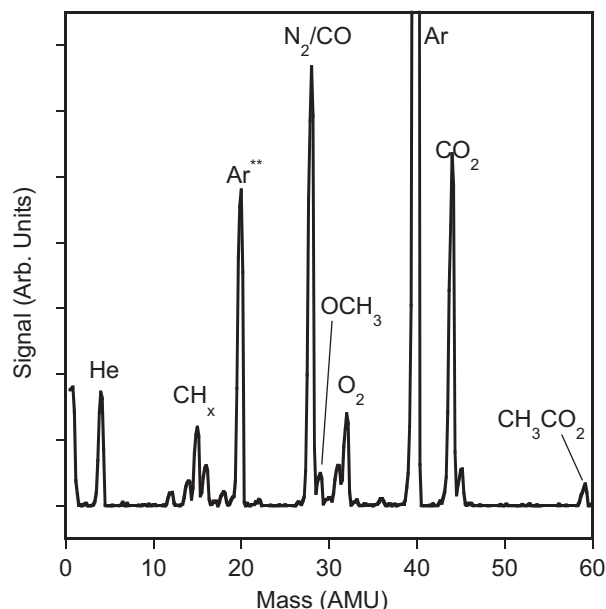


Fig. 3. Mass spectrometry data collected for the evolved gas Sample A.

### 3.3. Surface –OH chemistry

To estimate the acidity of the surface hydroxyls  $\text{NH}_3$ -TPD experiments were performed. Representative data are shown in Fig. S3. The TPD data indicates that there are no significant concentrations of acid groups on the surface of the  $\text{LiCoO}_2$  samples. The surface basicity was estimated by measuring the pH of the powder in water [26]. This pH data, Table 1, indicates that all the powders are slightly basic, with the most basic surface on the Sample C powder, likely due to  $\text{Li}_2\text{CO}_3$  discussed above. However, the magnitude of the basicity is similar indicating that this is not the origin of the observed activity. FTIR studies were attempted to characterize the surface hydroxyls further. However, due to the low concentrations and low surface area there is no evident OH's in the FTIR data, Fig. S4, making it at this point impossible to identify changes in reactivity due to surface protons.

### 3.4. Residual surface impurities

Elemental analysis from the XPS data indicated that all the cathode powders had residual sodium on their surfaces

( $\sim 1072$  eV), Table 1. This sodium likely originates from the starting source of Li used for the synthesis of  $\text{LiCoO}_2$ . Interestingly, the Sample A powder had the highest concentration of surface Na (5.5 at%) compared to the Sample C (0.5 at%) and Sample B materials (1.4 at%). In addition the Sample C and Sample B powders had 0.8 and 0.3 at% Ca on the surface.

This extensive analysis unfortunately did not identify a specific surface property that would explain the experimental results. We note that the most conclusive data indicates that the material with the most gas evolution is nearly stoichiometric and has the highest Na content. In contrast samples that deviate from ideal composition have virtually unmeasurable activities toward the decomposition of EC/DMC mixtures. How the excess Na on Sample A may differ from the excess Li in Sample C is not clear. If the reaction was simply attributed to surface salts (e.g.  $\text{Na}_2\text{CO}_3$ ,  $\text{Li}_2\text{CO}_3$ ) then Sample C should have an activity around 2.5 times less than Sample A. Identifying this surface chemistry, and ways to neutralize it, may enable the design of stable electrode configurations for long term storage or use.

To quantify the extent of electrolyte decomposition resulting in Coulombic irreversible capacities, the materials were fabricated

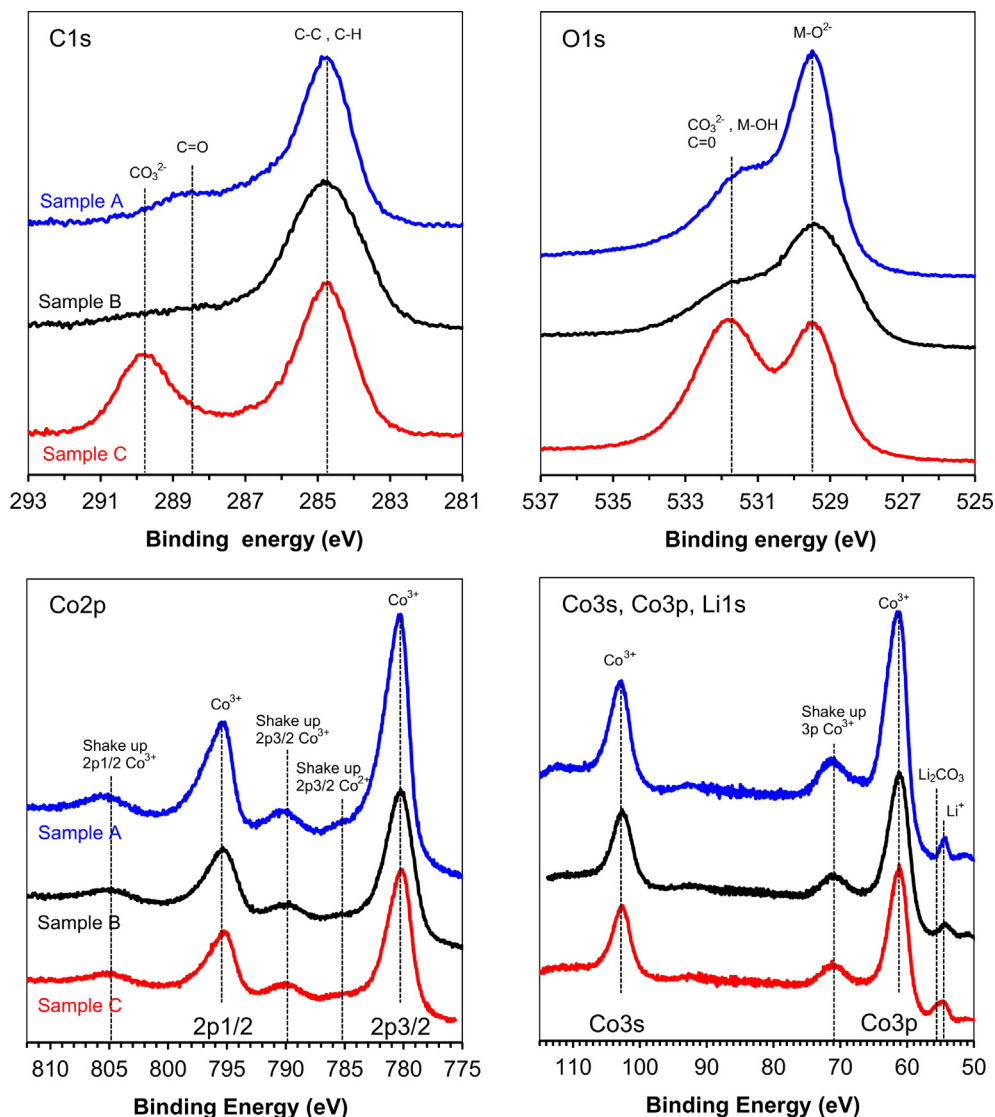


Fig. 4. High resolution XPS data collected for the pristine  $\text{LiCoO}_2$  powders.

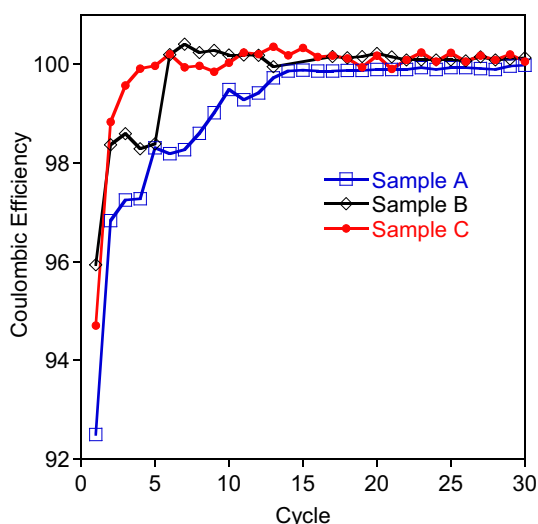


Fig. 5. Coulombic efficiency vs. cycle number when cycled against Li in 1.2 M LiPF<sub>6</sub>–EC/DMC (1:1 wt%).

into electrodes and cycled between 3 and 4.2 V vs. Li. Fig. 5 plots the Coulombic efficiency of these electrodes as a function of the first 30 cycles. The results show the Sample A material has the largest total irreversible capacity whereas the other materials rapidly deliver Coulombic efficiencies close to 100%. This larger irreversible capacity of the Sample A electrode may be correlated with the catalytic activity of the electrode. The surface sites may need to be reacted away or neutralized during cycling to prevent electrochemical losses. Identifying these sites should reduce initial capacity fading which occur with a number of electrode chemistries.

#### 4. Conclusion

An important aspect of these results may be the solubility of CO<sub>2</sub> in the electrolyte. It is conceivable that decomposing some of the electrolyte over the cathode surface would produce CO<sub>2</sub> which is dissolved in the remaining electrolyte. This CO<sub>2</sub> may react then at the anode surface aiding in the passivation reactions and SEI formation. If this hypothesis is true then adding CO<sub>2</sub> to an electrolyte may aid in the fabrication of more stable batteries. Another surprising aspect of this work is the strong effect of solvent composition on the observed gas evolution and CO<sub>2</sub> solubility. Likely, the molecular interactions between EC and DMC work to increase CO<sub>2</sub> solubility but also lower the activation energy to decomposition. The exact mechanism of this effect is unclear but will likely require advanced modeling and simulation to be identified. Finally, this work has focused on interactions with the solvents only. It is expected that the addition of a Li-salt, e.g. LiPF<sub>6</sub> or LiBF<sub>4</sub> will influence the observed properties. However, understanding these issues is crucial for better control reactions at the electrolyte–electrode interface. In addition, the decomposition of the solvent may produce insoluble species which deposit onto an electrode surface or participating in the SEI formation. This deposited species may be analyzed as SEI formation products, thus partially masking the actual electrochemical reactions forming the SEI.

#### Acknowledgments

This research was supported by the Materials Sciences and Engineering Division, Office of Basic Energy Sciences, U.S. Department of Energy under contract with UT-Battelle, LLC (KLB, LB, RRU, GMV) and the Fluid Interface Reactions, Structures, and Transport (FIRST) Center, an Energy Frontier Research Center funded by the U.S. Department of Energy, Office of Science, Office of Basic Energy Sciences (NJD). Experiments were conducted by KLB with assistance in cell design and data analysis by LB, GMV and NJD. A portion of the research was performed by Oak Ridge National Laboratory's ShaRE User Facility (SEM – RRU), which is sponsored by the Scientific User Facilities Division, Office of Basic Energy Sciences, U.S. Department of Energy.

#### Appendix A. Supplementary data

Supplementary data related to this article can be found at <http://dx.doi.org/10.1016/j.jpowsour.2013.03.118>.

#### References

- [1] D. Aurbach, K. Gamolsky, B. Markovsky, G. Salitra, Y. Gofer, U. Heider, R. Oesten, M. Schmidt, J. Electrochem. Soc. 147 (2000) 1322.
- [2] S.P.V. Nadimpalli, V.A. Sethuraman, S. Dalavi, B. Lucht, M.J. Chon, V.B. Shenoy, P.R. Guduru, J. Power Sources 215 (2012) 145.
- [3] K. Xu, Chem. Rev. 104 (2004) 4303.
- [4] J. Wolfenstine, D. Foster, W. Behl, S. Gilman, Gas Evolution and Self-discharge in Li/MnO<sub>2</sub> Primary Batteries, Army Research Laboratory, 1998.
- [5] A. Wuersig, W. Scheifele, P. Novák, J. Electrochem. Soc. 154 (2007) A449.
- [6] M. Onuki, S. Kinoshita, Y. Sakata, M. Yanagidate, Y. Otake, M. Ue, M. Deguchi, J. Electrochem. Soc. 155 (2008) A794.
- [7] W.H. Kong, H. Li, X.J. Huang, L.Q. Chen, J. Power Sources 142 (2005) 285.
- [8] K.H. Lee, E.H. Song, J.Y. Lee, B.H. Jung, H.S. Lim, J. Power Sources 132 (2004) 201.
- [9] S.E. Sloop, J.B. Kerr, K. Kinoshita, J. Power Sources 119 (2003) 330.
- [10] J. Vetter, M. Holzapfel, A. Wuersig, W. Scheifele, J. Uffheil, P. Novak, J. Power Sources 159 (2006) 277.
- [11] M.L. Machesky, D.A. Palmer, D.J. Wesolowski, Geochim. Cosmochim. Acta 58 (1994) 5627.
- [12] M.L. Machesky, M. Predota, D.J. Wesolowski, L. Vlcek, P.T. Cummings, J. Rosenqvist, M.K. Ridley, J.D. Kubicki, A.V. Bandura, N. Kumar, J.O. Sofo, Langmuir 24 (2008) 12331.
- [13] E. Mamontov, L. Vlcek, D.J. Wesolowski, P.T. Cummings, W. Wang, L.M. Anovitz, J. Rosenqvist, C.M. Brown, V.G. Sakai, J. Phys. Chem. C 111 (2007) 4328.
- [14] M. Predota, A.V. Bandura, P.T. Cummings, J.D. Kubicki, D.J. Wesolowski, A.A. Chialvo, M.L. Machesky, J. Phys. Chem. B 108 (2004) 12049.
- [15] D.R. Mullins, P.M. Albrecht, T.-L. Chen, F.C. Calaza, M.D. Biegalski, H.M. Christen, S.H. Overbury, J. Phys. Chem. C 116 (2012) 19419.
- [16] M. Gu, I. Belharouak, A. Genc, Z. Wang, D. Wang, K. Amine, F. Gao, G. Zhou, S. Thevuthasan, D.R. Baer, J.-G. Zhang, N.D. Browning, J. Liu, C. Wang, Nano Lett. 12 (2012) 5186.
- [17] S. Levasseur, M. Ménétrier, Y. Shao-Horn, L. Gautier, A. Audemer, G. Demazeau, A. Largeteau, C. Delmas, Chem. Mater. 15 (2002) 348.
- [18] D. Qian, Y. Hinuma, H. Chen, L.-S. Du, K.J. Carroll, G. Ceder, C.P. Grey, Y.S. Meng, J. Am. Chem. Soc. 134 (2012) 6096.
- [19] M. Ménétrier, D. Carlier, M. Blangero, C. Delmas, Electrochem. Solid State Lett. 11 (2008) A179.
- [20] R.J. Gummow, M.M. Thackeray, W.I.F. David, S. Hull, Mater. Res. Bull. 27 (1992) 327.
- [21] P. Kolář, H. Nakata, J.W. Shen, A. Tsuboi, H. Suzuki, A. Ue, Fluid Phase Equilibria 228 (2005) 59.
- [22] F. Blanchard, B. Carré, F. Bonhomme, P. Biensan, D. Lemordant, Can. J. Chem. 81 (2003) 385.
- [23] M. Anouti, Y.R. Dougassa, C. Tessier, L. El Ouatani, J. Jacquemin, J. Chem. Thermodyn. 50 (2012) 71.
- [24] G.M. Veith, A.R. Lupini, N.J. Dudney, J. Phys. Chem. C 113 (2009) 269.
- [25] G.M. Veith, J. Nanda, L.H. Delmau, N.J. Dudney, J. Phys. Chem. Lett. 3 (2012) 1242.
- [26] J.A. Singh, S.H. Overbury, N.J. Dudney, M. Li, G.M. Veith, ACS Catal. 2 (2012) 1138.